Journal of Zhejiang University-SCIENCE A (Applied Physics & Engineering)
ISSN 1673-565X (Print); ISSN 1862-1775 (Online)
www.jzus.zju.edu.cn; www.springerlink.com
E-mail: jzus@zju.edu.cn

Experimental investigation of nitrogen flow boiling heat transfer in a single mini-channel*

Bei-chen ZHANG[1,2], Qing-lian LI[1,2], Yuan WANG[†‡1,2],
Jian-qiang ZHANG[1,2], Jie SONG[1,2], Feng-chen ZHUANG[1,2,3]

[1]*Science and Technology on Scramjet Laboratory, National University of Defense Technology, Changsha 410073, China*
[2]*College of Aerospace Science and Engineering, National University of Defense Technology, Changsha 410073, China*
[3]*Space Engineering University, Beijing 101416, China*
[†]E-mail: ywangedi@outlook.com

Received Sept. 16, 2019; Revision accepted Dec. 27, 2019; Crosschecked Jan. 10, 2020

Abstract: Flow boiling heat transfer of nitrogen at high subcritical pressure conditions in a single vertical mini-channel with the diameter of 2.0 mm was experimentally investigated. The tested mass flux varied from 530 to 830 kg/(m^2·s), the inlet pressure ranged from 630 to 1080 kPa, and the heat flux ranged from 0 to 223.2 kW/m^2. Effects of the mass flux and the inlet pressure on the nitrogen boiling curve were examined. Results showed that within the limited test conditions, the merging of three boiling curves indicates the dominance of nucleate boiling and the inlet pressure has a positive enhancement on heat transfer performance. Three heat transfer trends were identified with increasing heat flux. At low heat fluxes, the heat transfer coefficient increases first and then decreases with vapour quality. At intermediate heat fluxes, the heat transfer coefficient versus the vapour quality presents an inverted "U" shape. At high heat fluxes, a double valley shape was observed and the partial dry-out in intermittent flow and annular flow helps to interpret the phenomenon. The increasing inlet pressure increases the heat transfer coefficient over a wide range of vapour quality until the partial dry-out inception. The lower surface tension and lower latent heat of evaporation enhance the nucleate boiling for higher inlet pressure. A modified experimental correlation (mean absolute error (MAE)=19.3%) was proposed on the basis of the Tran correlation considering both the nucleate boiling and the partial dry-out heat transfer mechanism.

Key words: Mini-channel; Nitrogen; Flow boiling; Heat transfer; Regenerative cooling
https://doi.org/10.1631/jzus.A1900468 **CLC number:** V41

1 Introduction

Liquid oxygen/methane is a promising candidate for future exploration with in-situ propellant production, improved performance, improved reusability and elimination of toxicity issues for surface operations, and fluid commonality (Hurlbert et al., 2016) in reaction control engines and main engines. Regenerative cooling has been identified as one of the technology gaps. This refers to where one of the propellants is circulated through cooling passages inside the chamber wall before it is provided to the injection head (Huzel and Huang, 1992; Sutton, 2005). It was reported that Northrop Grumman put forward a reaction control engine concept where the thrust chamber and the throat were regeneratively cooled with both oxygen and methane (Klem et al., 2011). This effectively enhanced engine performance. However, the application of phase-change heat transfer of cryogenic propellant in mini-channels to regenerative cooling of a rocket engine has scarcely been studied. As a safe alternative working fluid, liquid nitrogen has similar thermophysical properties to liquid methane and/or oxygen and was used to study the heat

‡ Corresponding author
* Project supported by the National Natural Science Foundation of China (No. 11872373)
ORCID: Yuan WANG, https://orcid.org/0000-0001-5724-555X

transfer process and characteristics of vertical mini-channel flow boiling under high pressure.

Extensive studies have been conducted on mini/micro-channel flow boiling heat transfer. As schematically presented by Kim and Mudawar (2013, 2014), the two dominant heat transfer mechanisms in mini/micro-channel are nucleate boiling and convective boiling, respectively. In fact, the actual heat transfer mechanisms in mini/micro-channel is much more complex than the two mechanisms (Thome and Consolini, 2010; Cheng and Xia, 2017). Recently, a lot of efforts have been carried out on the effects of channel geometry (Shahmardan et al., 2012; Li et al., 2017; Lee et al., 2018; Liu et al., 2018), working fluids (Sempértegui-Tapia and Ribatski, 2017; Huang et al., 2018; Sandler et al., 2018; Yang et al., 2018), and the operating conditions (especially the saturation pressure) (Charnay et al., 2014, 2015) on the two-phase heat transfer mechanisms in mini/micro-channels (Cheng and Xia, 2017; Karayiannis and Mahmoud, 2017). However, the heat transfer mechanisms and characteristics were insufficient for cryogenic fluids. Compared with conventional fluids, cryogenic fluids have some unique thermophysical properties. The comparison of some commonly used conventional fluids and cryogenic fluids at 1000 kPa saturation pressure is given in Table 1. As can be seen, because of the low liquid-gas density ratio of nitrogen, a homogeneous model can be used to predict the pressure drop of nitrogen two-phase flow (Qi, 2007). In addition, since nucleated bubbles are attached to the heating wall by surface tension, the decreased dominance of surface tension for cryogenic fluids contributes to the departure of the bubbles from the heating wall. This means that the bubbles can be easily created and depart with smaller bubble size at lower surface tension (Fang et al., 2016; Zhang et al., 2017). For nitrogen and oxygen, the latent heat of evaporation is relatively low, so the vapour quality of flow boiling changes rapidly along the tube (Qi, 2007). These thermophysical properties would influence the nitrogen flow boiling heat transfer both in macro- and mini-/micro-channels.

Flow boiling of nitrogen in macro-channels has been investigated over the last decades (Laverty and Rohsenow, 1964; Steiner and Schlünder, 1976; Klimenko, 1982; Umekawa et al., 2002; Yu, 2012; Wang and Fang, 2014; Fang et al., 2016, 2019). A unique phenomenon of nitrogen upward flow in vertical macro-channels was reported by several researchers. It has been accepted that the main heat transfer mechanism in macro-channels is nucleate boiling, and/or the conjugate nucleate and convective boiling.

Laverty and Rohsenow (1964) were among the earliest researchers conducting nitrogen flow boiling heat transfer and visualized experiments. Four flow patterns were identified as well as two peaks and one valley, forming a V-shape, in terms of heat transfer coefficient versus vapour quality. The phenomenon was frequently observed in nitrogen upward flow boiling in a vertical 14 mm stainless steel tube (Yu, 2012). It was explained that between the first peak and the valley, i.e. the left side of the V-shape, the nucleated boiling dominated. After the valley, however, the heat transfer coefficient first increases due to the enhancement of convection effect and then decreases after the second peak for the vapor layer appearing between the tube wall and the liquid.

Recently, Wang and Fang (2014) and Fang et al. (2016, 2019) thoroughly studied nitrogen flow boiling heat transfer and critical heat flux (CHF) in a macro-channel. A detailed analysis on the V-shape between two CHF points was conducted in terms of thermophysical properties and flow orientation. Among the two CHF points, one is the departure of nucleate boiling (DNB)-type that occurs at low vapour quality and is most likely caused by the bubble crowding mechanism, and the other is the dry-out-type that appears at high vapour quality and is caused by liquid deficiency in the flow. It is found that the Fang correlation (Fang, 2013) has the best prediction performance among the six selected correlations.

Steiner and Schlünder (1976) carried out an experimental study of liquid nitrogen flow boiling heat transfer in a smooth horizontal copper tube with 14 mm inner diameter. The mass flux varies from 40 to 450 kg/(m^2·s), working fluid inlet pressure from 500 to 1600 kPa, heat flux from 0.3 to 40 kW/m^2, and vapour quality from 0.02 to 1. Results showed that the heat transfer coefficient depends on the heat flux as well as the mass flux. The effects of vapour quality could not be neglected. Forced convective evaporation was not observed and the dominant heat transfer mechanism was nucleate boiling.

Table 1 Thermophysical property comparison of cryogenic and conventional fluids at p_{sat}=1000 kPa

Fluid		T_{sat} (K)	ρ_L (kg/m^3)	ρ_V (kg/m^3)	ρ_L/ρ_V	σ (mN/m)	h_{fg} (kJ/kg)
Conventional	Water	453.03	887.13	5.15	172.42	42.22	2014.60
	Ethanol	423.85	647.20	15.25	42.45	7.24	685.69
	R22	296.57	1196.80	42.34	28.27	8.30	184.30
Cryogenic	Nitrogen	103.75	665.83	41.33	16.11	3.33	152.06
	Methane	149.14	359.62	15.70	22.91	5.34	415.66
	Oxygen	119.62	976.34	38.46	25.39	6.22	174.34

p_{sat} is the saturation pressure; T_{sat} is the saturation temperature; ρ_L and ρ_V are the liquid phase density and vapour phase density, respectively; σ is the surface tension; h_{fg} is the latent heat of evaporation

In (Klimenko, 1982), the nitrogen flow boiling heat transfer data were compared with the Chen correlation (Chen, 1963) and the Shah correlation (Shah, 1976). It was found that the Shah correlation gives a two- or three-fold underestimation of the value of heat transfer coefficients, while the Chen correlation gives mainly underestimated values of the heat transfer coefficients with a mean absolute error (MAE) of 200% in the high heat flux region. Based on the data from nine references, Klimenko (1982) proposed a correlation on cryogenic liquid (nitrogen, hydrogen, and neon) forced flow boiling heat transfer. A modified boiling number was proposed. This refers to the transition point for distinguishing nucleate boiling from forced convective evaporation.

Umekawa et al. (2002) carried out heat transfer experiments on the downward flow of liquid nitrogen in a 5 mm stainless steel tube with mass flux from 147 to 465 kg/(m^2·s), inlet pressure of 100 kPa, heat flux from 2 to 21.5 kW/m^2, and vapour quality less than 0.2. It was found that the Steiner correlation (Steiner, 1986) could predict the experimental results well.

For mini/micro-channel flow boiling, limited studies were carried out based on a survey on the open literature, among which the tested inlet pressures were at a relative low level.

A series of heat transfer and visualization experiments on the flow boiling of liquid nitrogen were conducted in vertical mini-/micro-channels (Qi et al., 2007a, 2007b; Fu et al., 2008, 2010; Zhang and Fu, 2009). Qi et al. (2007a, 2007b) studied liquid nitrogen flow boiling in 0.531, 0.834, 1.042, and 1.931 mm channels, focusing on the onset of nucleate, two-phase flow instability, two-phase pressure drop, convective heat transfer coefficient, and critical heat flux. For the 0.531–1.042 mm micro-channels, a new correlation considering both nucleate boiling and convective evaporation was proposed in terms of the confinement number *Co*, the boiling number *Bo*, the Weber number *We*, the dimensionless pressure number K_p, and the Lockhart-Martinelli number *X*. While for the 1.931 mm channel, it was found that the Chen correlation (Chen, 1963) has a good agreement with the test data and the heat transfer coefficient increases with vapour quality in the convection evaporation dominant region, so the diameter of 1.931 mm seems to fall into the range of macro-channel, which is different from the results using conventional fluids (Huo et al., 2004; Tibiriçá and Ribatski, 2010).

In recent years, systematic studies were conducted on nitrogen flow boiling CHF (Liu et al., 2017), instability (Chen et al., 2018), and the heat transfer characteristics (Zhang et al., 2017; Chen et al., 2019) in horizontal small/mini-channels. The overall inlet pressure varies from 192 to 420 kPa, mass flux from 170 to 690 kg/(m^2·s), heat flux from 1.4 to 67.1 kW/m^2, and vapour quality from 0 to 0.81. For the 1.98 mm channel, it was found that nucleate boiling dominates at low vapour quality while convective evaporation dominates in the intermediate-to-high vapour quality region. Based on the experimental data of 1.98 mm and 2.92 mm channels, a modified correlation was proposed considering both nucleate boiling and convective evaporation mechanisms. The comparison with the literature data showed that the proposed correlation has good prediction accuracy on flow boiling in the small horizontal channels, but the deviations could be large for that in the vertical channels.

Hartwig et al. (2015, 2016) and Mercado et al. (2019) conducted a serial research on cryogenic

quenching and flow boiling correlation assessment in both macro-channels and mini-channels. It was found that there exists large discrepancies between the experimental data and the predicted values, as many of the correlations were developed for conventional fluids, not cryogens. So the flow boiling and heat transfer characteristics of liquid nitrogen in mini-channels still need to be further explored and the experimental database requires to be further enlarged.

Considering the practical application background, it is necessary to carry out further nitrogen flow boiling tests under similar conditions of the engine regenerative cooling processes. Specifically, we aim to explore the cryogenic fluid flow boiling characteristics under high pressure, the study of which, according to the existing literature, has been very limited. As shown in Table 2, when the saturation pressure increases, the surface tension and the latent heat of evaporation decrease. Such variations of properties result in an intensification of the nucleate boiling heat transfer due to an increase of the number of active nucleation sites and to a decrease of the detachment bubble radius, which increases bubble frequency and reduces bubble size (Charnay et al., 2015). A low surface tension and latent heat of vaporization tend to quick evaporation, which facilitates the generation of bubbles (Fang et al., 2016). On the other hand, the convective boiling contribution is not sufficient at high saturation pressure. Indeed, the density of the vapour increases with saturation pressure, thereby its velocity decreases. Moreover, the liquid film conductivity decreases with increasing saturation pressure. Thus, the conduction and the convection through the liquid film are reduced and, as a consequence, the contribution of the convective boiling is reduced at high saturation pressure (Charnay et al., 2015). The differences brought by the variation of conditions should be highlighted.

Table 2 Nitrogen thermo physical property at p_{sat}=100, 500, and 1000 kPa

p_{sat} (kPa)	ρ_L (kg/m^3)	ρ_V (kg/m^3)	k_L (mW/(m·K))	σ (mN/m)	h_{fg} (kJ/kg)
100	806.59	4.56	144.99	8.90	199.32
500	723.80	20.65	111.93	5.25	173.32
1000	665.83	41.33	92.738	3.33	152.06

k_L is the coefficient of thermal conductivity

According to a previous review, experimental study on nitrogen flow boiling is still limited and needs further study. The present study conducted experiments of nitrogen flow boiling in a vertical mini-channel at high pressure (630–1080 kPa) in order to determine the heat transfer mechanism of liquid nitrogen under high pressure and verify the experimental correlation. Effects of heat flux, inlet pressure, and mass flux on the boiling curve and heat transfer coefficient were discussed and analyzed to better understand the heat transfer mechanism of nitrogen flow boiling in a vertical mini-channel. The experimental results were compared against six existing correlations and a modified correlation was proposed based on the experimental data. The obtained experimental heat transfer relationship will be used to improve the accuracy of regenerative cooling modeling and guide the design of a regenerative cooling passage.

2 Experimental system and test section

An integrated experimental system was designed and calibrated to investigate the nitrogen flow boiling heat transfer characteristics in a mini-channel. This includes the gas nitrogen source (GN_2), the self-pressurization nitrogen storage tank (low pressure LN_2), the vacuum Dewar, the high pressure nitrogen storage tank (high pressure LN_2), the test section, the evaporator, the sonic nozzle, the direct current (DC) power, and the data acquisition system, as shown in Fig. 1a. To reduce heat leakage from the ambient, both the high-pressure storage tank and the test section are installed in the vacuum Dewar. Before the test begins, the vacuum Dewar is evacuated to 1×10^{-3} Pa by the two-stage-vacuum-pump (not shown in Fig. 1a) and precooled to ~77 K by nitrogen forced convection. The steady nitrogen single-phase flow is established through three procedures. The first is the filling and precooling of the high pressure LN_2 tank. The low pressure LN_2 is pressured into the high-pressure nitrogen storage tank by self-pressurization constantly until the high-pressure storage tank is full. The second procedure is the precooling of the test section. The liquid nitrogen is pressured through the test section and then evaporates completely through the evaporator. The gas nitrogen is exhausted to the

atmosphere after flowing through the supersonic nozzle. Finally, the mass flow rate and inlet pressure of the test section are controlled by adjusting the GN_2 pressure reducer, the diameter of the venturi tube, and the diameter of the supersonic nozzle. The mass flow rate of the gas nitrogen is measured by the Endress +Hauser® PROMASS 80 (Germany) mass flow meter with an accuracy of ±0.15%. The test section is then heated by Joule heating directly to obtain the single-phase and two-phase heat transfer data. The effective heating voltage on the test section, the mass flow rate, temperature, and pressure signals were recorded synchronously by the NI® PXIe-1073 (USA) data acquisition system with an acquisition frequency of 10 Hz through the aviation plugs in the steady state. Based on a frequency analysis of the temperature, pressure, and mass flow rate profile in single-phase liquid nitrogen flow, the investigated flow in the present study could be considered as stable flow and heat transfer process.

Fig. 1b illustrates the schematic drawing of the test section, which consists of the mini-channel, the connecting pipe, and the electrode. Circular high-precision 321 stainless steel was used as the mini-channel. To measure the outer surface temperatures, ten 0.25 mm T-type thermocouples T_{w1}–T_{w10} were welded to the mini-channel at the desired longitudinal locations z_1–z_{10} (Table 3) with the temperature accuracy of ±0.5 K. The thermal contacting resistance is ignored in the present study due to the welding process. The mini-channel was welded to the connecting pipes (material: 304 stainless steel) with the fluid temperature and pressure transducer connectors. The connecting pipes have the same inner diameter as the mini-channel so as to try to avoid the pressure loss caused by the sudden contraction and expansion. $T_{f,in}$ and $T_{f,out}$ were the fluid temperatures at the inlet and outlet of the test section, respectively. The fluid temperatures were measured by thermal resistance detector (RTD) with a measurement accuracy of ±0.5 K. The RTD was calibrated by the Technical Institute of Physics and Chemistry, China. The inlet and outlet pressures p_{in} and p_{out} were measured by Hefei Zhongya SENSOR® PT301 pressure transducers with a range of 0–2.0 MPa and an accuracy of ±0.5% full scale. The electrode is used to connect the test section with the DC power through copper electrode connections at the top of the vacuum Dewar. The effective voltage applied to the mini-channel was measured by the NI® PXIe 4300 (USA) with an accuracy of 0.15% and the current was recorded directly by the DC power (pawer® DPSP 1000 (China)) with an accuracy of 0.5% full scale. The effective heat power was evaluated though a single-phase gas nitrogen test in the vacuum Dewar, which will be presented in Section 3.1.

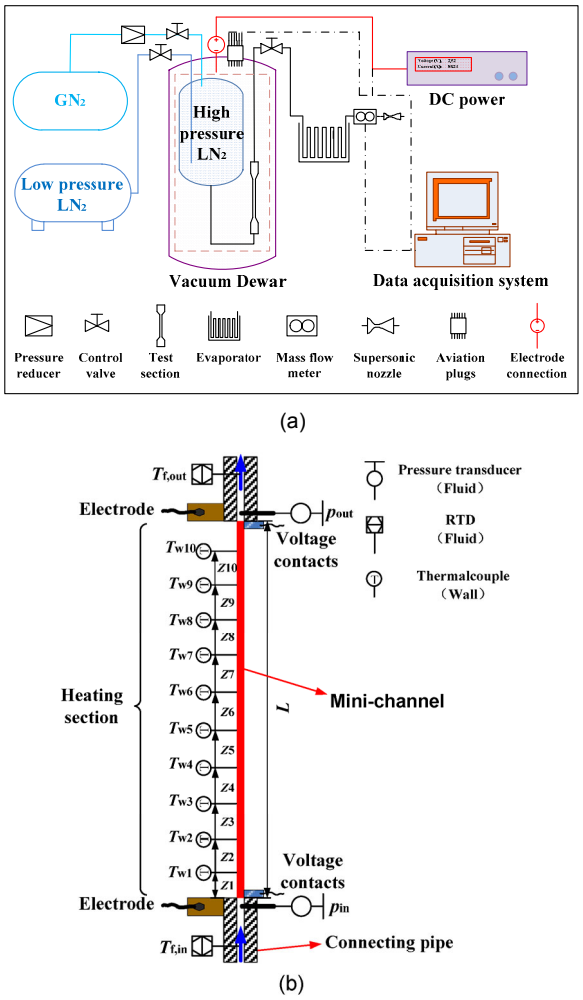

Fig. 1 Schematic drawing of the experimental system (a) and the test section (b)

L is the length of the channel

The inner diameter of the mini-channel is 2.0 mm with an inner diameter measurement accuracy of ±0.01 mm. The mini-channel inner surface roughness e was analysed by Talysurf PGI 1240®. The ratio of inner surface roughness to inner diameter e/D_i is 0.0036. Table 4 gives the geometry parameters of the mini-channel.

Table 3 Locations of thermocouples of the mini-channel

Parameter	Value	Parameter	Value
z_1 (mm)	13.8	z_6 (mm)	168.1
z_2 (mm)	44.4	z_7 (mm)	197.5
z_3 (mm)	76.1	z_8 (mm)	228.2
z_4 (mm)	106.4	z_9 (mm)	259.6
z_5 (mm)	136.6	z_{10} (mm)	289.5

Table 4 Geometry parameters of the mini-channel

Item	Description	Item	Description
Material	321 stainless steel	L (mm)	296.31
D_i (mm)	2	e (mm)	7.16×10^{-3}
D_o (mm)	4	e/D_i	0.0036

D_i and D_o are the inner and outer diameters of the channel, respectively; L is the length of the channel; e is the inner surface roughness of the channel

3 Data reduction

3.1 Effective heat flux

The total heat power Q_{tot} is computed as $Q_{tot}=UI$, where U and I are the effective heating voltage and current, respectively.

The single-phase gas nitrogen heat transfer test is conducted in the vacuum Dewar to obtain the effective heat power Q_{eff}, which is calculated as

$$Q_{eff}=\dot{m}c_p(T_{f,out}-T_{f,in}), \tag{1}$$

where $\dot{m}$ is the mass flow rate, and c_p is the specific heat.

The relationship between Q_{eff} and Q_{tot} is shown in Fig. 2 and fitted as

$$Q_{eff}=0.989Q_{tot}. \tag{2}$$

The effective heat flux q is calculated as

$$q=\frac{Q_{eff}}{A_i}, \tag{3}$$

where the inner surface area of the mini-channel $A_i=\pi D_i L$.

The mass flux G is calculated as

$$G=\frac{\dot{m}}{A_c}, \tag{4}$$

where the cross-sectional area of the mini-channel $A_c=\pi/4\times D_i^2$.

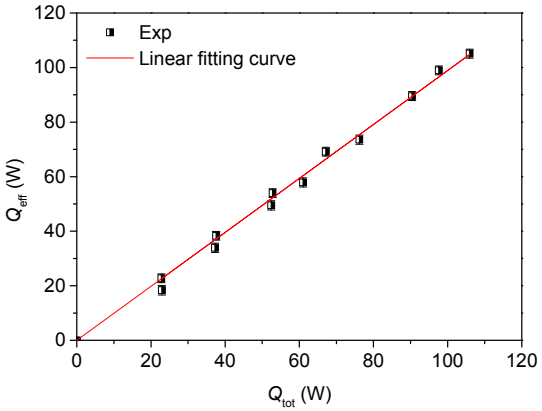

Fig. 2 Effective heat power versus total heat power in nitrogen gas test (Exp)

3.2 Average heat transfer coefficient

The average heat transfer coefficient h_{avg} is calculated as

$$h_{avg}=\frac{q}{T_{wi,avg}-T_{f,avg}}, \tag{5}$$

where the average wall temperature $T_{wi,avg}$ is defined as

$$T_{wi,avg}=\frac{\sum_{j=1}^{10}T_{wi,j}}{10}, \tag{6}$$

and the average fluid temperature $T_{f,avg}$ is the arithmetic average value of $T_{f,in}$ and $T_{f,out}$.

The Nusselt number Nu is calculated as

$$Nu=\frac{h_{avg}D_i}{k_L}, \tag{7}$$

where k_L is the thermal conductivity of the fluid.

3.3 Local heat transfer coefficient and the vapour quality

The local heat transfer coefficient h is calculated as

$$h=\frac{q}{T_{wi,j}-T_{f,z}}, \tag{8}$$

where $T_{wi,j}$ is the internal wall temperature and $T_{f,z}$ is the bulk mean temperature at the measurement location.

According to the heat conduction equation with the internal heating source, the internal wall temperature $T_{\mathrm{wi},j}$ is calculated based on the measured outer wall temperature $T_{\mathrm{wo},j}$:

$$T_{\mathrm{wi},j}=T_{\mathrm{wo},j}+\frac{q_{\mathrm{v}}}{4k_{\mathrm{w}}}\left[\left(\frac{D_{\mathrm{o}}}{2}\right)^2-\left(\frac{D_{\mathrm{i}}}{2}\right)^2\right]+\left(\frac{q}{k_{\mathrm{w}}}\frac{D_{\mathrm{i}}}{2}+\frac{q_{\mathrm{v}}}{2k_{\mathrm{w}}}\left(\frac{D_{\mathrm{i}}}{2}\right)^2\right)\ln\frac{D_{\mathrm{o}}}{D_{\mathrm{i}}},\tag{9}$$

where k_{w} is the thermal conductivity of the wall, and q_{v} is the heat flux per volume, which is calculated as

$$q_{\mathrm{v}}=\frac{Q_{\mathrm{eff}}}{\frac{\pi}{4}(D_{\mathrm{o}}^2-D_{\mathrm{i}}^2)L}.\tag{10}$$

To prevent the liquid nitrogen from evaporating before entering the mini-channel, the liquid nitrogen usually maintains a certain degree of subcooling. Therefore, there is a single-phase subcooling section in the mini-channel. By iteratively solving the single-phase heat balance Eq. (11), single-phase pressure drop Eq. (12) and searching the saturated pressure Eq. (13) through the NIST® software, the length of subcooling L_{sub} is obtained.

$$T_{\mathrm{f},z}=T_{\mathrm{f,in}}+\frac{4qL_{\mathrm{sub}}}{GD_{\mathrm{i}}c_{\mathrm{p}}},\tag{11}$$

$$p_z=p_{\mathrm{in}}-f\frac{G^2}{2\rho_{\mathrm{L}}}\frac{L_{\mathrm{sub}}}{D_{\mathrm{i}}},\tag{12}$$

$$T_{\mathrm{f},z}=T_{\mathrm{f,sat}}(p_z),\tag{13}$$

where the single-phase friction factor f is calculated based on the Colebrook correlation (Qi, 2007).

The bulk mean temperature at the measurement location $T_{\mathrm{f},z}$ is calculated by Eq. (14). When the longitudinal location $z<L_{\mathrm{sub}}$, the fluid bulk temperature is calculated by the single-phase heat balance equation, and when $z\geq L_{\mathrm{sub}}$, the fluid bulk temperature is the saturated temperature $T_{\mathrm{f,sat}}$ under the local pressure based on the NIST® software.

$$T_{\mathrm{f},z}=\begin{cases}T_{\mathrm{f,in}}+\dfrac{4qz}{GD_{\mathrm{i}}c_{\mathrm{p}}}, & z<L_{\mathrm{sub}},\\ T_{\mathrm{f,sat}}(p_z), & z\geq L_{\mathrm{sub}},\end{cases}\tag{14}$$

where the local pressure p_z is calculated based on the pressure drop calculation, which consists of the total single-phase pressure drop and the corresponding two-phase pressure drop.

The two-phase pressure drop gradient along the mini-channel consists of three components, i.e. the friction, acceleration, and gravitation pressure drop gradients,

$$\frac{\mathrm{d}p}{\mathrm{d}z}=\frac{\mathrm{d}p_{\mathrm{f}}}{\mathrm{d}z}+\frac{\mathrm{d}p_{\mathrm{a}}}{\mathrm{d}z}+\frac{\mathrm{d}p_{\mathrm{g}}}{\mathrm{d}z},\tag{15}$$

where the friction, acceleration, and gravitation pressure drop gradient components are calculated based on the homogeneous model (Qi, 2007).

$$\frac{\mathrm{d}p_{\mathrm{f}}}{\mathrm{d}z}=f_{\mathrm{tp}}\frac{G^2}{2\rho_{\mathrm{tp}}}\frac{1}{D_{\mathrm{i}}},\tag{16}$$

$$\frac{\mathrm{d}p_{\mathrm{a}}}{\mathrm{d}z}=\frac{\mathrm{d}}{\mathrm{d}z}\left\{G^2\left[\frac{(1-x)^2}{\rho_{\mathrm{L}}(1-\varepsilon)}+\frac{x^2}{\rho_{\mathrm{V}}\varepsilon}\right]\right\},\tag{17}$$

$$\frac{\mathrm{d}p_{\mathrm{g}}}{\mathrm{d}z}=[\rho_{\mathrm{V}}\varepsilon+\rho_{\mathrm{L}}(1-\varepsilon)]g,\tag{18}$$

where g is the gravitational acceleration, the two-phase fraction factor f_{tp} is determined by the Colebrook correlation (Qi, 2007), and the two-phase density ρ_{tp} is calculated by

$$\rho_{\mathrm{tp}}=\frac{\rho_{\mathrm{L}}\rho_{\mathrm{V}}}{\rho_{\mathrm{V}}(1-x)+\rho_{\mathrm{L}}x}.\tag{19}$$

The void friction ε is determined by

$$\varepsilon=\frac{\rho_{\mathrm{L}}/\rho_{\mathrm{V}}}{1/x+(\rho_{\mathrm{L}}/\rho_{\mathrm{V}}-1)}.\tag{20}$$

The local thermodynamic equilibrium vapour quality x is calculated as

$$x=\frac{q\pi D_{\mathrm{i}}(z-L_{\mathrm{sub}})}{\dot{m}h_{\mathrm{fg}}}.\tag{21}$$

Due to the small pressure drop in 2.0 mm channel, the flash vapour quality is neglected in the present study.

3.4 Uncertainty analysis

The experimental uncertainties mainly came from the channel dimension, the mass flow rate, the heat power, and the temperature measurements. According to the standard uncertainty analysis of Taylor (1997), uncertainties of mini-channel inner diameter, channel length, inner surface area, mass flow rate, mass flux, effective heat power, effective heat flux, and heat transfer coefficient were estimated. Maximum uncertainties are summarized in Table 5.

Table 5 Maximum uncertainties

Parameter	Maximum uncertainty (%)
Mini-channel inner diameter	0.5
Mini-channel length	0.0067
Inner surface area	0.5
Mass flow rate	0.15
Mass flux	1.01
Voltage	0.15
Current	0.5
Effective heat power	0.52
Effective heat flux	0.72
Heat transfer coefficient	10.07

4 Flow boiling experimental results

4.1 Single-phase heat transfer validation

The single-phase liquid nitrogen heat transfer validation is conducted in the channel with D_i=2.0 mm under a variety of Reynolds conditions. Fig. 3 gives the single-phase Nusselt number Nu versus Reynolds number Re ranging from 7985 to 14323. The Dittus-Boelter correlation Eq. (22) and the Gnielinski correlation Eq. (23) were used to validate the experimental data. Both correlations are applied to the heat transfer in fully developed turbulent flow in smooth tubes. It is noted that the applicable Re of the Dittus-Boelter correlation is over 10000, while the applicable Re of the Gnielinski correlation is from 2300 to 1×10^6.

$$Nu = 0.023Re^{0.8}Pr^{0.4}, \tag{22}$$

$$Nu = \frac{(f/8)(Re-1000)Pr}{1+12.7\sqrt{f/8}\left(Pr^{2/3}-1\right)}, \tag{23}$$

where Pr is the Prandtl number and f is the single-phase friction factor, calculated by the Filonenko correlation:

$$f = (1.82\lg Re - 1.64)^{-2}. \tag{24}$$

As shown in Fig. 3, the experimental Nusselt numbers increase with Reynolds numbers and the experimental data show good agreement with the Gnielinski correlation, within ±15%. It is also found that the prediction of the Dittus-Boelter correlation is similar to the Gnielinski correlation at the condition of Re>10000. The single-phase result helps to validate the experimental system, procedure, and data reduction employed in this study.

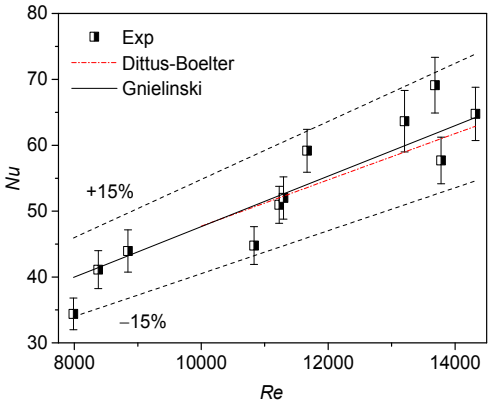

Fig. 3 Single-phase Nusselt number versus Reynolds number (D_i=2.0 mm)

4.2 Boiling curves

The flow boiling curves for nitrogen at three different mass fluxes and three different inlet pressures were obtained as plotted in Fig. 4 and Fig. 5, respectively. The plot shows the variation of wall superheat at the downstream location T_{w9} with the heat flux. The heat flux ranges from 0 to 223.2 kW/m^2 until the CHF is reached.

As represented in Fig. 4, at a wall superheat of 8–10 K, there is a sharp change in slope of the curves marking the onset of nucleate boiling (ONB). It can also be seen that the heat flux of ONB increases with the mass flux. After the ONB, the wall superheat becomes less sensitive to heat flux as the fluid begins to consume the latent heat (Balasubramanian et al., 2011). According to Wang and Sefiane (2012), the increase in the slopes of the boiling curves is caused by the transition from partial nucleate boiling to fully

developed nucleate boiling. It is found that the boiling curves at different mass fluxes collapse beyond the ONB, which might be caused by the narrow range of mass flux. Besides, the merging of the boiling curves at the limited range of test conditions indicates the dominance of nucleate boiling according to Bertsch et al. (2008) and Harirchian and Garimella (2008). However, the CHF at G=830 kg/(m^2·s) did not increase as expected, the reason for which is most likely related to the increasing inlet pressure due to the control accuracy of the inlet pressure.

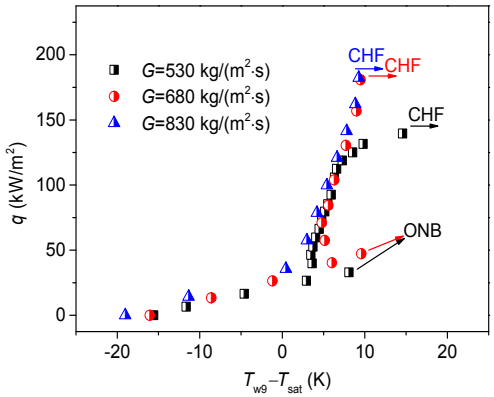

Fig. 4 Effect of mass flux on boiling curves (D_i=2.0 mm, p_{in}=630–740 kPa)

Note that the "hysteresis phenomenon" occurs at a mass flux of 530 kg/(m^2·s) and 680 kg/(m^2·s), which means at the sudden fall of temperature after the ONB. Qi et al. (2007b) also found the temperature hysteresis phenomenon and considered that it was caused by the transition from single-phase forced convection to two-phase flow boiling. A more prevalent view is that the decrease of wall superheat required for nucleation of residual gases results in a significant drop in wall temperature.

The effect of the inlet pressure on boiling curves is shown in Fig. 5. It is found that the effect of pressure on ONB should be highlighted. The higher the pressure, the lower the wall superheat required for ONB. The superheat for bubble nucleation decreases with increasing saturation pressure, which is in concert with Zhang et al. (2017) and Chen et al. (2019). Different from Fig. 4, the effect of the inlet pressure on the boiling curve could be identified after the ONB. With the increase of inlet pressure, the wall superheat decreases at the same heat flux, which indicates that the increase of the inlet pressure has a positive enhancement on heat transfer performance.

Note that the CHF decreases with the increase of inlet pressure. The higher the pressure, the easier heat transfer deterioration will occur. The possible reason for this will be discussed in Section 4.3.4 and further study is still needed on this phenomenon.

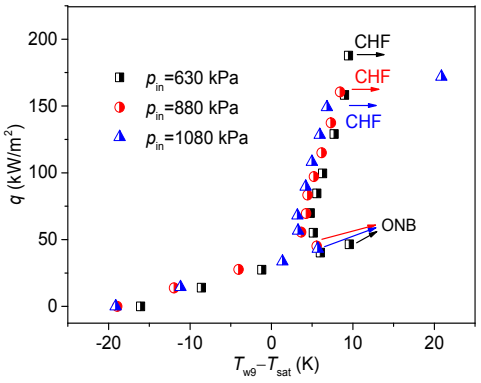

Fig. 5 Effect of inlet pressure on boiling curves (D_i= 2.0 mm, and G=680 kg/(m^2·s))

4.3 Heat transfer coefficients versus vapour quality

4.3.1 Flow patterns

Four flow patterns are identified in the present experimental investigation: intermittent, annular, dry-out, and mist flows. According to the nitrogen flow pattern visualization in 1.931 mm mini-channel conducted by Fu et al. (2008), the bubbly, slug, and churn flows could be grouped together in intermittent flow. The nucleate boiling, thin film evaporation of the liquid film trapped between the bubble and the wall and the convection to the liquid and vapour slugs between two successive bubbles are the most important heat transfer mechanisms (Thome and Consolini, 2010). Different from the annular flow described by Fang et al. (2016), in mini-channel annular flow, the vapour phase becomes a continuous flow in the core of the channel and is surrounded by a thin liquid film (Fu et al., 2008). The conduction and convective evaporation across the liquid film should be the dominant heat transfer mechanism. According to Charnay et al. (2014), the dry-out flow regime corresponds to the regime that starts when the liquid film disappears at the wall partially and/or intermittently, and lasts until the inception of the mist flow

where the liquid film is entrained into the high velocity vapour core with or without redeposition on the channel walls. To help better understand the heat transfer dominant mechanisms at high saturation pressures, the transition between intermittent flow (IF) and annular flow (AF) is indicated by a black line in the following sections.

4.3.2 Influence of heat flux on heat transfer coefficient versus vapour quality

The influence of the heat flux over the heat transfer coefficient is illustrated on Fig. 6 for an inlet pressure of 630 kPa and for a mass flux of 530 kg/(m^2·s). In general, the higher the heat flux, the larger the heat transfer coefficient. Three heat transfer trends can be identified with the increasing heat flux.

At low and intermediate heat fluxes (59.7 kW/m^2 ≤q≤118.8 kW/m^2), for low vapour quality the heat transfer coefficient increases with vapour quality and raises slightly with heat flux during the intermittent flow regime. It is clear that small bubbles play an important role in conditions of low quality (Charnay et al., 2015). Indeed, the properties of nitrogen, e.g. the lower surface tension and the lower latent heat of evaporation (Table 1), result in an intensification of the nucleate boiling heat transfer due to an increase of the number of active nucleation sites and to a decrease of the detachment bubble radius, which means the bubbles could be easily created and depart with smaller bubble sizes in liquid nitrogen (Charnay et al., 2015; Zhang et al., 2017). Thus, the slight increase of heat flux would have little enhancement on nucleation boiling under low and intermediate heat flux conditions. At higher vapour quality, for low heat fluxes, the heat transfer coefficient decreases with the vapour quality. However, for intermediate heat fluxes, the heat transfer coefficient versus vapor quality has a characteristic of an inverted "U" shape and increases little with heat flux. When the flow pattern becomes annular, the heat transfer coefficient decreases slightly at first and then falls sharply with increasing vapour quality. On one hand, the decrease of the heat transfer coefficient results from the reduction of the nucleate boiling contribution in the annular flow regime. On the other hand, it was found that the deposition of the liquid droplets could cause the decrease of the heat transfer coefficient (Qu and Mudawar, 2003) in annular flow. In addition, Dupont et al. (2004) suggested that the liquid film partial dry-out could also cause the heat transfer coefficient decline.

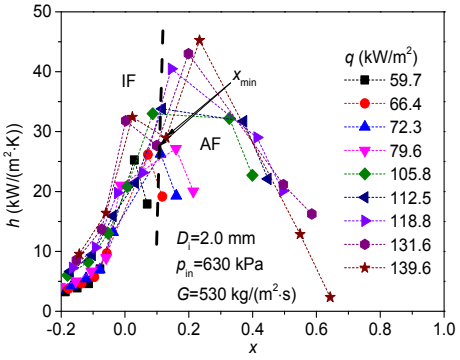

Fig. 6 Influence of heat flux on the heat transfer coefficient. D_i=2.0 mm, p_{in}=630 kPa, and G=530 kg/(m^2·s)

At higher heat fluxes (q≥131.6 kW/m^2), the heat transfer coefficient first decreases, then increases to the peak and finally decreases with the vapour quality. This produces a unique double valley shape. For low vapour quality, nucleate boiling is the dominant heat transfer mechanism. Because of the properties of the nitrogen, a large number of small bubbles tend to coalesce into intermittent flow at high heat flux. Thereby, the percentage of the vapour convection (partial dry-out) of the intermittent flow increases and results in the decrease of the heat transfer coefficient (Thome and Consolini, 2010). The curves exhibit a minimum heat transfer coefficient value which coincides with the intermittent-annular flow pattern transition. The vapour quality corresponding to the minimum value of heat transfer coefficient is called x_{min}. For vapour quality higher than x_{min}, the annular liquid film becomes thinner and the convective evaporation contribution is sufficient to lead to an increase of the heat transfer coefficient with increasing vapor quality. However, after the heat transfer coefficient reaches the peak, the heat transfer coefficient falls sharply. This corresponds to the partial dry-out inception of the liquid film (Fang et al., 2016), indicating the occurrence of the dry-out flow.

Fig. 7 highlights the influence of heat flux on the heat transfer coefficient at a similar inlet pressure of 665 kPa and higher mass flux of 680 kg/(m^2·s). At higher mass flux, it is clear that the higher the heat flux, the larger the heat transfer coefficient and three heat transfer trends could still be identified. However, it was found that the nucleation boiling contribution is

suppressed at low vapour quality under higher mass flux, for the double valley shape not only exists at higher heat fluxes (187.8 kW/m^2≤q≤223.2 kW/m^2) but also appears when it comes to intermediate heat fluxes (129.0 kW/m^2≤q≤158.2 kW/m^2).

At intermediate heat flux conditions (129.0 kW/m^2≤q≤158.2 kW/m^2), for low vapour quality, the heat transfer coefficient decreases abruptly with increasing vapour quality during intermittent flow. In the previous analysis of Section 4.2, it was found that the higher the mass flux, the larger the wall superheat required for ONB, leading to a decrease of the number of active nucleation sites. Therefore, the nucleate boiling is suppressed during intermittent flow at higher mass flux. After the x_{min}, the heat transfer coefficient marks out a plateau resulting from the decrease of nucleate boiling and the increase of convective evaporation when it comes to the annular flow. For higher vapour quality, the heat transfer coefficient falls with increasing vapour quality, corresponding to the inception of partial dry-out.

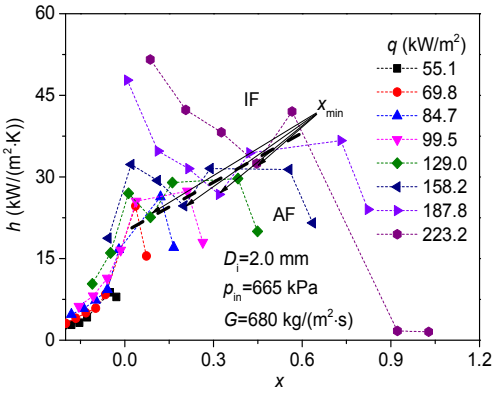

Fig. 7 Influence of heat flux on the heat transfer coefficient. D_i=2.0 mm, p_{in}=665 kPa, G=680 kg/(m^2·s)

At higher heat flux conditions (q≥187.8 kW/m^2), for the lower vapour quality region, the heat transfer is mainly due to nucleate boiling and the heat transfer coefficient decreases sharply corresponding to the intermittent flow regime. The bubbles tend to coalesce to form bigger bubbles, and as a consequence, it suggests that this abrupt decrease was most likely caused by partial dry-out during intermittent flow. For higher vapour qualities, the heat transfer coefficient increases with increasing vapour quality until the inception of dry-out flow. The completion of dry-out flow indicates that the mist flow and the heat transfer coefficient become nearly constant in value in this regime.

Fig. 8 represents the influence of the heat flux on the heat transfer coefficient for two higher inlet pressures: p_{in}=890 kPa (Fig. 8a) and p_{in}=1000 kPa (Fig. 8b), at a constant mass flux (680 kg/(m^2·s)). Under higher inlet pressure, the three heat transfer trends are no longer apparent with increasing heat flux, especially for p_{in}=1000 kPa. This means that the influence of the heat flux on the heat transfer coefficient is weakened at higher inlet pressure.

For an inlet pressure of 890 kPa (Fig. 8a), the heat flux has little influence on the heat transfer coefficient over the vapour quality range for low and intermittent heat fluxes while the heat flux increases the heat transfer coefficient at higher heat fluxes.

At low and intermediate heat fluxes (83.4 kW/m^2≤q≤160.5 kW/m^2), for low vapour quality, the heat transfer coefficient increases with increasing vapour quality during intermittent flow. This means that the nucleate boiling contribution to heat transfer is enhanced again with increasing inlet pressure. For inlet pressure of 890 kPa, nucleate boiling is enhanced and the increase of heat flux cannot influence the heat transfer coefficient under low and intermediate heat fluxes.

At higher heat fluxes (q≥186.8 kW/m^2), the double valley shape only exists when the heat flux increases to 211.7 kW/m^2. At the highest heat flux, the intense nucleate boiling causes the small bubbles to coalesce in the intermittent flow and the decrease of the heat transfer coefficient. Surpassing the x_{min}, the convective evaporation of the annular film increases the heat transfer coefficient. Furthermore, the partial dry-out of the annular flow liquid film causes the decrease of the heat transfer coefficient.

For an inlet pressure of 1000 kPa (Fig. 8b), the influence of the heat flux on the heat transfer coefficient is not significant. Indeed, at higher saturation pressure, the bubble detachment diameter is smaller and the bubble frequency is higher because of the modification of nitrogen thermophysical properties (Table 2). The nucleate boiling contribution to heat transfer is extremely intense under high inlet pressure. Thus, the influence of increase of heat flux on the heat transfer coefficient is not obvious. It is found that neither the inverted "U" shape nor the double valley shape occurred (Fig. 8b), indicating that the heat

transfer coefficient is a weak function of the vapour quality at high inlet pressure.

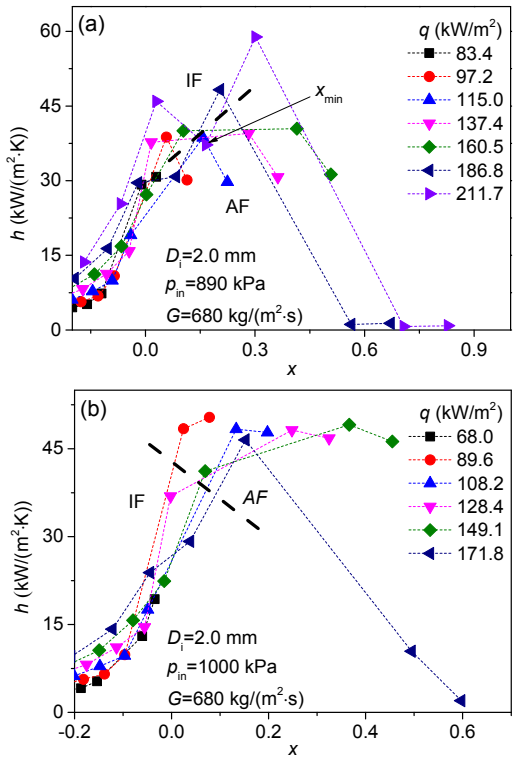

Fig. 8 Influence of heat flux on the heat transfer coefficient: (a) p_{in}=890 kPa; (b) p_{in}=1000 kPa. D_i=2.0 mm, G=680 kg/(m^2·s)

4.3.3 Influence of mass flux on heat transfer coefficient versus vapour quality

Mass flux is one of the physical parameters that the most strongly affects the heat transfer in convective boiling. For flow boiling in mini/micro-channels, both mass flux and heat flux can affect the boiling process significantly, depending on the channel sizes and shapes, fluid type, and operation conditions. Nucleate boiling and convective boiling heat transfer are the two dominant heat transfer mechanisms in micro-scale channels. However, the actual heat transfer mechanisms in micro-channels are much more complex than the two mechanisms. (Kim and Mudawar, 2014; Cheng and Xia, 2017) The influence of the mass flux on heat transfer coefficient depends on the experimental conditions.

Fig. 9 shows the effects of mass flux on heat transfer coefficient at the inlet pressure of 630 kPa at two heat flux conditions: q=125.1 kW/m^2 (Fig. 9a) and q=158.2 kW/m^2 (Fig. 9b). At low vapour quality (during intermittent flow), the nucleate boiling is enlightened due to the modification of the nitrogen properties at the tested higher inlet pressure condition and the nucleate boiling becomes the dominant mechanism. It is shown that the heat transfer coefficient decreases with the increasing vapour quality and decreases with the increasing mass flux, which indicates that the increase of the mass flux suppresses the nucleate boiling.

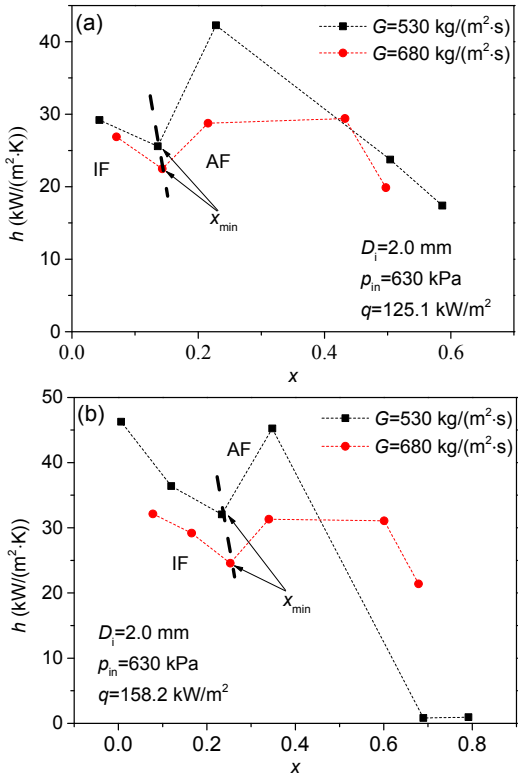

Fig. 9 Influence of mass flux on the heat transfer coefficient: (a) q=125.1 kW/m^2; (b) q=158.2 kW/m^2. D_i=2.0 mm, p_{in}=630 kPa

After x_{min}, which corresponds to the annular flow, the increase of mass flux decreases the heat transfer coefficient within the limited mass flux conditions. In annular flow, the liquid film thickness increases with the mass flux before the dry-out occurs. However, with the dry-out occurring on the liquid film, the heat transfer coefficient decreases with the vapour quality at mass flux of 530 kg/(m^2·s) condition. The increase of the mass flux postpones the dry-out and the heat transfer coefficient is higher with the larger mass flux after the dry-out occurs (Fig. 9b).

As Agostini et al. (2008) and Ribatski et al. (2006) illustrated, in most cases, the heat transfer

coefficient increases with increasing mass flux; however, other variations are also observed, which reflects the complicity of the flow boiling mechanism in micro/mini-channels.

4.3.4 Influence of inlet pressure on heat transfer coefficient versus vapour quality

Major modifications are expected when varying the inlet pressure from 665 to 1000 kPa. Indeed, some modifications in properties at high inlet pressure strongly enhance the nucleation boiling contribution to heat transfer, leading to an increase of the heat transfer coefficient. Fig. 10 highlights the influence of the inlet pressure at a constant mass flux (680 kg/(m^2·s)) for two different heat fluxes: q=158.2 kW/m^2 (Fig. 10a) and q=186.7 kW/m^2 (Fig. 10b). The higher the inlet pressure, the larger the heat transfer coefficient is over a wide range of vapour quality until the inception of partial dry-out.

As shown in Fig. 10, the heat transfer coefficient increases with increasing inlet pressure. This is in accordance with the previous analysis of the boiling curve. According to Bao et al. (2000) and Qi et al. (2007b), the reason for this is related to the superheat degree decreasing with the increase of pressure in the nucleate boiling region. In addition, the bubble frequency is higher and the bubble size is smaller with the increase of inlet pressure. This facilitates the decreased range of intermittent flow and the earlier transition to the annular flow. Because of the enhancement of nucleate boiling, this results in an overall increase of the heat transfer coefficient.

In Fig. 10b, the increase of the inlet pressure leads to the earlier occurrence of partial dry-out. The reason for this is related to the modification of nitrogen thermophysical properties. The higher the saturation pressure, the smaller the surface tension, which plays an important role in maintaining the annular film steady. The lower the surface tension, the higher the liquid film entrainment fraction (droplets) is. As a consequence, the annular film could be unsteady under higher inlet pressure and the partial dry-out would occur earlier.

4.4 Heat transfer correlation assessment

Experimental heat transfer results were compared with six existing correlations (Chen (1963), Shah (1976), Klimenko (1982), Tran et al. (1996), Qi et al. (2007b), and Kim and Mudawar (2013)) for macro-, mini-, and micro-channels. The Chen and Shah correlations are widely used in the macro-channel heat transfer calculation. The Chen correlation considers the addition of the nucleate and convective boiling contribution. Although the Chen correlation is based on conventional fluids, Butterworth and Hewitt (1977) and Clark (1969) suggested that the Chen correlation is suitable for the cryogenic fluid. The Klimenko correlation is based on cryogenic fluids and validated by the nitrogen experimental data (Klimenko and Sudarchikov, 1983), which considers the nucleate boiling and the convective evaporation by a modified Bo^*. The main heat transfer mechanism of the Tran correlation was nucleate boiling and it has been validated by the nitrogen flow boiling data (Zhang et al., 2017; Chen et al., 2019). The Qi correlation is based on the nitrogen data obtained in micro-channels, consisting of both nucleate and convective boiling. The Kim-Mudawar correlation is proposed based on the superposition of nucleate boiling and convective boiling for refrigerants, CO_2, and water. The details of selected correlations are summarized in Table 6.

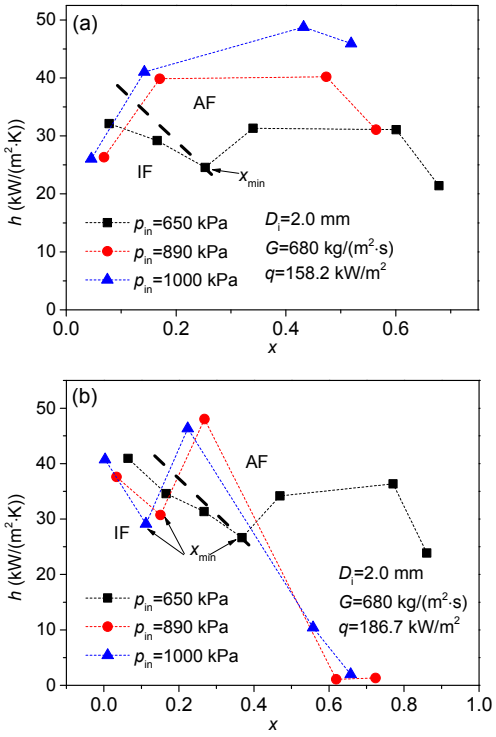

Fig. 10 Influence of inlet pressure on the heat transfer coefficient: (a) q=158.2 kW/m^2; (b) q=186.7 kW/m^2. D_i=2.0 mm, G=680 kg/(m^2·s)

Table 6 Summary of selected correlations for saturated flow boiling heat transfer in macro-, mini-, and micro-channels

Reference	Parameter range	Correlation for heat transfer coefficient
Chen, 1963	Water and organic fluids: p=56–3228 kPa, x=0.01–0.71, macro-channels and annulus	$h_{tp}=Eh_L+Sh_{nb}$, $h_L=0.023(Re_L)^{0.8}(Pr_L)^{0.4}(k_L/D_i)$, $h_{nb}=0.00122\left(\dfrac{k_L^{0.79}c_{pL}^{0.45}\rho_L^{0.49}}{\sigma^{0.5}\mu_L^{0.29}h_{fg}^{0.24}\rho_V^{0.24}}\right)^{0.8}(\Delta T_{sat})^{0.24}(\Delta p)^{0.75}$, $E=(1+1/X^{0.5})^{1.78}$, $S=0.9622-0.5822\left[\arctan\left(\dfrac{Re_LF^{1.25}}{6.18\times10^4}\right)\right]$, $X=\left(\dfrac{1-x}{x}\right)^{0.9}\left(\dfrac{\rho_V}{\rho_L}\right)^{0.5}\left(\dfrac{\mu_L}{\mu_V}\right)^{0.1}$, $Re_L=\dfrac{G(1-x)D_i}{\mu_L}$, $Pr_L=\dfrac{c_{pL}\mu_L}{k_L}$
Shah, 1976	Water and refrigerants (R11, R22, R12, R502): D_i=5–15.8 mm, G=70–11071 kg/(m^2·s), q=90–1215 kW/m^2, x=0–0.7, macro-channels	$h_{tp}=\max(E,S)h_L$, $h_L=0.023(Re_L)^{0.8}(Pr_L)^{0.4}(k_L/D_i)$, $\begin{cases}S=1.8/N^{0.8},\ E=230Bo^{0.5}, & N>1.0,\\ S=1.8/N^{0.8},\ E=FBo^{0.5}\exp(2.74N^{-0.1}), & 0.1<N\le1.0,\\ S=1.8/N^{0.8},\ E=FBo^{0.5}\exp(2.47N^{-0.15}), & N\le0.1,\end{cases}$ $\begin{cases}F=14.70, & Bo\ge1.1\times10^{-3},\\ F=15.43, & Bo<1.1\times10^{-3},\end{cases}$ $N=\left(\dfrac{1-x}{x}\right)^{0.8}\left(\dfrac{\rho_V}{\rho_L}\right)^{0.5}$, $Bo=q/(h_{fg}G)$
Klimenko, 1982	Nitrogen: D_i=1.6–14.1 mm, p=90–2200 kPa G=20–2200 kg/(m^2·s) q=0.4–210 kW/m^2	$Nu/Nu_L=\begin{cases}1, & Bo_*^{0.5}<6\times10^4,\\ 0.0041Bo_*^{0.5}, & Bo_*^{0.5}\ge6\times10^4,\end{cases}$ $Nu=\dfrac{hb}{k_L}$, $b=\left[\sigma/g(\rho_L-\rho_V)\right]^{0.5}$, $Bo_*=\dfrac{h_{fg}G}{q}\left[1+x(\rho_L/\rho_V-1)\right]$, $Nu_L=0.0042Pe_*^{0.6}K_p^{0.5}K_s^{0.2}$, $Pe_*=qb/(h_{fg}\rho_Va)$, $K_p=p/[\sigma g(\rho_L-\rho_V)]^{0.5}$, $K_s=\dfrac{(\rho c_pk)_w}{(\rho c_pk)_L}$
Tran et al., 1996	R12: D_i=2.4–2.92 mm, p=510, 820 kPa, G=44–832 kg/(m^2·s), q=3.6–129 kW/m^2, x=0–0.94	$h_{tp}=8.4\times10^5(Bo^2We_L)^{0.3}\left(\dfrac{\rho_L}{\rho_V}\right)^{-0.4}$, $We_L=\dfrac{G^2D_i}{\rho_L\sigma}$
Qi et al., 2007a	Nitrogen: D_i=0.531, 0.834, 1.042 mm, G=440–3000 kg/(m^2·s), q=50–213 kW/m^2	$\begin{cases}Nu=1059.83Bo^{0.454}We^{0.045}K_p^{0.106}X^{0.107}Co^{-1.825}, & x<0.3,\\ Nu=0.0042Bo^{-0.872}We^{-0.059}K_p^{0.293}X^{0.065}Co^{-1.704}, & x\ge0.3,\end{cases}$ $Co=\sqrt{\sigma/[(\rho_L-\rho_V)gD_i^2]}$
Kim and Mudawar, 2013	Refrigerants, CO_2, and water: D_i=0.19–6.5 mm, p_R=0.005–0.69, G=19–1608 kg/(m^2·s), x=0–1	$h_{tp}=\sqrt{h_{nb}^2+h_{cb}^2}$, $p_R=p/p_{crit}$, $h_{nb}=\left[2345\left(Bo\dfrac{P_H}{P_F}\right)^{0.7}p_R^{0.38}(1-x)-0.51\right](0.023Re_L^{0.8}Pr_L^{0.4}k_L/D_i)$, $h_{cb}=\left[5.2\left(Bo\dfrac{P_H}{P_F}\right)^{0.08}We_L^{-0.54}+3.5\left(\dfrac{1}{X}\right)^{0.94}\left(\dfrac{\rho_V}{\rho_L}\right)^{0.25}\right](0.023Re_L^{0.8}Pr_L^{0.4}k_L/D_i)$

h_{tp}: two-phase heat transfer coefficient; h_L: liquid phase heat transfer coefficient; h_{nb}: nucleate boiling heat transfer coefficient; c_{pL}: liquid phase specific heat; ΔT_{sat}: wall superheat; Δp: pressure drop corresponding to the wall superheat; E: enhancement factor; S: suppression factor; X: Lockhart-Martinelli number; μ_L: liquid phase viscosity; μ_V: vapour phase viscosity; Re_L: liquid phase Reynolds number; Pr_L: liquid phase Prandtl number; N: dimensionless parameter in Shah correlation; Bo: boiling number; E: function of Bo and N in Shah correlation; S: function of N in Shah correlation; F: parameter defined in Shah correlation; Nu_L: liquid phase Nusselt number; b: Laplace constant; Bo^*: modified Boiling number; Pe_*: modified Peclet number; a: thermal diffusivity; K_p: dimensionless pressure number; K_s: dimensionless surface number; ρ_w: wall material density; c_{pw}: wall material specific heat; k_w: wall material thermal conductivity; Co: confinement number; We_L: liquid phase Weber number; h_{cb}: convective boiling dominant heat transfer coefficient; P_H: heated perimeter of channel; P_F: wetted perimeter of channel; p_R: reduced pressure; p_{crit}: critical pressure

Figs. 11a–11f show the ratios of the calculated to experimental heat transfer coefficient plotted against the vapour quality based on the Chen, Shah, Klimenko, Tran, Qi, and Kim-Mudawar correlations, respectively. The predictive accuracy of correlations is evaluated by the mean absolute error (MAE), which is defined as

$$\mathrm{MAE}=\frac{\sum\left(\left|h_{\mathrm{exp}}-h_{\mathrm{cal}}\right|/h_{\mathrm{exp}}\right)}{M}\times 100\%, \tag{25}$$

where M is the number of data points.

In Fig. 11, ratios of the calculated heat transfer coefficient to the experimental heat transfer coefficient show an increasing trend when the vapour quality exceeds 0.6 for all the six correlations. Specifically, the Chen correlation overestimates the heat transfer coefficient in the case of low vapour quality (for vapour quality less than 0.2), while the Shah correlation overestimates the heat transfer coefficient over the whole vapour quality range. It can be seen from Figs. 11c and 11d that the Klimenko and Tran correlations can estimate the heat transfer coefficient with the vapour quality well when the vapour quality

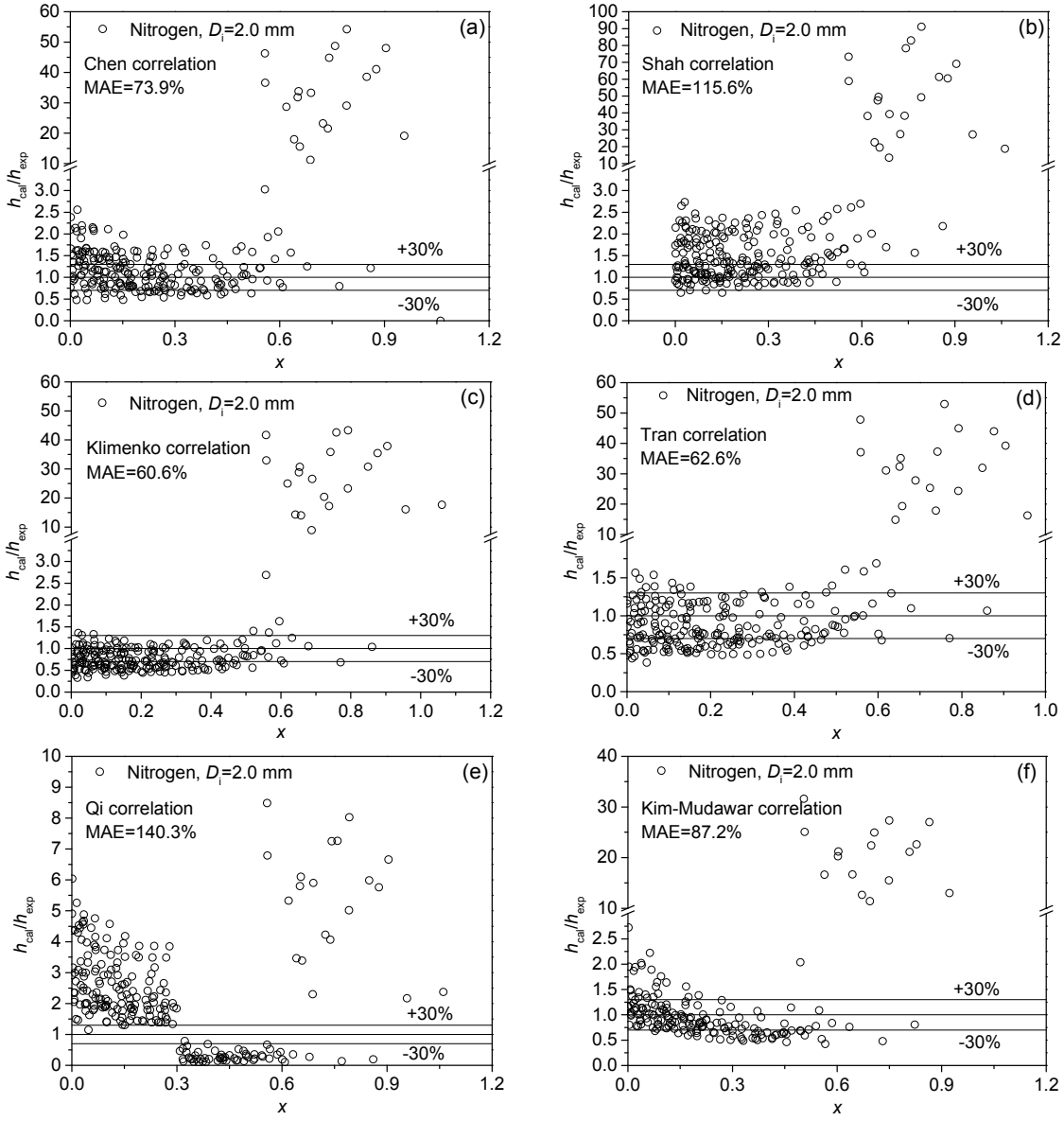

Fig. 11 Ratios of the calculated to experimental heat transfer coefficient versus vapour quality
(a) Chen; (b) Shah; (c) Klimenko; (d) Tran; (e) Qi; (f) Kim-Mudawar

is less than 0.6. The Qi correlation overestimated the heat transfer coefficient at x<0.3 while it underestimated the data when x≥0.3, which suggests that the 2.0 mm channel might not be for the micro-scale range. For the Kim-Mudawar correlation, the discrepancy is mainly concentrated in the low vapour quality region and the region with vapour quality greater than 0.6. Table 7 gives MAEs of selected correlations.

As shown in Fig. 11 and Table 7, the Klimenko and the Tran correlations have better MAEs (60.6% and 62.6%, respectively) among the six selected correlations. However, the Klimenko and Tran correlations could not predict the heat transfer coefficient well when x≥0.6, where the partial dry-out causes heat transfer deterioration. Thus, a modified correlation needs to be proposed, taking into account both the nucleate boiling and dry-out heat transfer mechanism. The Tran correlation considers the effects of heat flux against flow heat capacity (Bo), flow inertia against liquid surface tension (We_L), and the fluid character (ρ_L/ρ_V), which represents the dominant heat transfer mechanism of nucleation boiling (Zhang et al., 2017). Based on the formation of the Tran correlation, the Lockhart-Martinelli number X and the dimensionless pressure number K_p are also considered in the modified correlation, which are rewritten as shown in Table 8.

As can be seen in Fig. 12, the modified correlation agrees well with the experimental data and an MAE of ±19.3% is obtained in experimental conditions. This means that the modified correlation considering the nucleate boiling and the partial dry-out heat transfer gives a relatively good description of the experimental data. More experiments are conducted to further investigate the nitrogen heat transfer mechanism and validate the correlation.

5 Conclusions

The flow boiling heat transfer of nitrogen at high subcritical pressure in a single vertical mini-channel was experimentally investigated. The tested mass flux was varied from 530 to 830 kg/(m^2·s), the inlet pressure from 630 to 1080 kPa, and the heat flux from 0 to 223.2 kW/m^2. Effects of the heat flux, inlet pressure and mass flux on the boiling curve, and the heat transfer coefficient were discussed and analyzed to better understand the heat transfer mechanism of

Table 7 Summary of MAEs of selected correlations and the modified correlation

Selected correlation	MAE (%)
Macro-channel correlations	
Chen	73.9
Shah	115.6
Klimenko	60.6
Mini- and micro-channel correlations	
Tran	62.6
Qi	140.3
Kim-Mudawar	87.2
Modified correlation	19.3

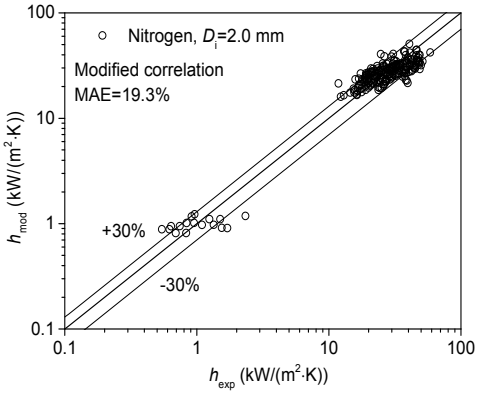

Fig. 12 Comparison of experimental heat transfer coefficient data with the modified correlation

Table 8 Modified correlation for nitrogen flow boiling heat transfer

Parameter range	Correlation for heat transfer coefficient
Nitrogen: single mini-channel, D_i=2.0 mm, p_{in}=630–1080 kPa, G=530–830 kg/(m^2·s), q=0–230 kW/m^2, x=0–1	$\begin{cases} Nu = 12.46Bo^{0.544}We^{0.035}X^{0.031}K_p^{0.614}, & x < 0.6, \\ Nu = 0.00136Bo^{-1.442}We^{0.074}, & x \geq 0.6, \end{cases}$ $Bo = q/(h_{fg}G),\ We_L = \dfrac{G^2 D_i}{\rho_L \sigma},\ X = \left(\dfrac{1-x}{x}\right)^{0.9}\left(\dfrac{\rho_V}{\rho_L}\right)^{0.5}\left(\dfrac{\mu_L}{\mu_V}\right)^{0.1},$ $K_p = p/[\sigma g(\rho_L - \rho_V)]^{0.5}$

nitrogen flow boiling under high saturation pressures in a vertical mini-channel. The experimental results were compared against six predictive correlations and a modified correlation was proposed based on the experimental data. From this study, the following conclusions can be drawn:

1. Within the limited test conditions, the merging of three boiling curves indicates the dominance of nucleate boiling. Besides, the increasing mass flux helps to enhance the CHF. The increase of the inlet pressure has a positive enhancement on the heat transfer performance. The CHF decreases with the increase of inlet pressure.

2. The heat flux has a dramatic effect on the heat transfer coefficient. Three heat transfer trends were identified with increasing heat flux. At low heat flux, the heat transfer coefficient first increases and then decreases with the vapour quality. At intermediate heat flux, the heat transfer coefficient presents an inverted "U" shape and is dependent on the heat flux. At high heat flux, the double valley shape was observed and the reason for this is that it corresponds to the partial dry-out in the intermittent flow and the annular flow. At higher mass flux, the nucleation boiling is suppressed and the double valley shape appears at intermediate heat flux. At higher inlet pressure, the influence of the heat flux and the vapour quality on the heat transfer coefficient is weakened because of the modification of nitrogen properties with saturation pressure.

3. Within the limited mass flux conditions, the increase of mass flux suppresses the nucleate boiling contribution to the heat transfer during intermittent flow. In annular flow, the increase of mass flux increases the annular film thickness and decreases the heat transfer coefficient before dry-out occurs.

4. The increasing inlet pressure increases the heat transfer coefficient over a wide range of vapour quality until the inception of partial dry-out. The lower surface tension and lower latent heat of evaporation enhance the nucleate boiling for higher inlet pressures. The increase of inlet pressure leads to the earlier occurrence of the partial dry-out, with the reason for this related to the unsteady liquid film with a lower surface tension under high inlet pressure.

5. It was found that the Klimenko and Tran correlations have better prediction accuracies among the six selected correlations. A modified correlation (MAE=19.3%) was proposed on the basis of the Tran correlation considering both nucleate boiling and the partial dry-out heat transfer mechanism.

Contributors

Qing-lian LI, Yuan WANG, and Feng-chen ZHUANG designed the research. Jian-qiang ZHANG and Jie SONG processed the corresponding data. Bei-chen ZHANG and Jie SONG wrote the first draft of the manuscript. Qing-lian LI and Yuan WANG helped to organize the manuscript. Qing-lian LI, Yuan WANG, and Bei-chen ZHANG revised and edited the final version.

Conflict of interest

Bei-chen ZHANG, Qing-lian LI, Yuan WANG, Jian-qiang ZHANG, Jie SONG, and Feng-chen ZHUANG declare that they have no conflict of interest.

References

Agostini B, Thome JR, Fabbri M, et al., 2008. High heat flux flow boiling in silicon multi-microchannels–part I: heat transfer characteristics of refrigerant R236fa. *International Journal of Heat and Mass Transfer*, 51(21-22): 5400-5414. https://doi.org/10.1016/j.ijheatmasstransfer.2008.03.006

Balasubramanian K, Lee PS, Jin LW, et al., 2011. Experimental investigations of flow boiling heat transfer and pressure drop in straight and expanding microchannels–a comparative study. *International Journal of Thermal Sciences*, 50(12):2413-2421. https://doi.org/10.1016/j.ijthermalsci.2011.07.007

Bao ZY, Fletcher DF, Haynes BS, 2000. Flow boiling heat transfer of Freon R11 and HCFC123 in narrow passages. *International Journal of Heat and Mass Transfer*, 43(18): 3347-3358. https://doi.org/10.1016/S0017-9310(99)00379-8

Bertsch SS, Groll EA, Garimella SV, 2008. Refrigerant flow boiling heat transfer in parallel microchannels as a function of local vapor quality. *International Journal of Heat and Mass Transfer*, 51(19-20):4775-4787. https://doi.org/10.1016/j.ijheatmasstransfer.2008.01.026

Butterworth D, Hewitt GF, 1977. Two-phase Flow and Heat Transfer. Oxford University Press, UK.

Charnay R, Revellin R, Bonjour J, 2014. Flow boiling characteristics of R-245fa in a minichannel at medium saturation temperatures. *Experimental Thermal and Fluid Science*, 59:184-194. https://doi.org/10.1016/j.expthermflusci.2014.01.011

Charnay R, Revellin R, Bonjour J, 2015. Flow boiling heat transfer in minichannels at high saturation temperatures: Part I–experimental investigation and analysis of the heat transfer mechanisms. *International Journal of Heat and Mass Transfer*, 87:636-652. https://doi.org/10.1016/j.ijheatmasstransfer.2015.03.081

Chen JC, 1963. A correlation for boiling heat transfer to saturated fluids in convective flow. Heat Transfer Conference, p.11-14.

Chen ST, Chen XY, Luo GQ, et al., 2018. Flow boiling instability of liquid nitrogen in horizontal mini channels. *Applied Thermal Engineering*, 144:812-824. https://doi.org/10.1016/j.applthermaleng.2018.08.100

Chen ST, Chen XY, Chen L, et al., 2019. Experimental study on the heat transfer characteristics of saturated liquid nitrogen flow boiling in small-diameter horizontal tubes. *Experimental Thermal and Fluid Science*, 101:27-36. https://doi.org/10.1016/j.expthermflusci.2018.09.020

Cheng LX, Xia GD, 2017. Fundamental issues, mechanisms and models of flow boiling heat transfer in microscale channels. *International Journal of Heat and Mass Transfer*, 108:97-127. https://doi.org/10.1016/j.ijheatmasstransfer.2016.12.003

Clark JA, 1969. Cryogenic heat transfer. *Advances in Heat Transfer*, 5:325-517. https://doi.org/10.1016/S0065-2717(08)70132-1

Dupont V, Thome JR, Jacobi AM, 2004. Heat transfer model for evaporation in microchannels. Part II: comparison with the database. *International Journal of Heat and Mass Transfer*, 47(14-16):3387-3401. https://doi.org/10.1016/j.ijheatmasstransfer.2004.01.007

Fang XD, 2013. A new correlation of flow boiling heat transfer coefficients based on R134a data. *International Journal of Heat and Mass Transfer*, 66:279-283. https://doi.org/10.1016/j.ijheatmasstransfer.2013.07.015

Fang XD, Sudarchikov AM, Chen YF, et al., 2016. Experimental investigation of saturated flow boiling heat transfer of nitrogen in a macro-tube. *International Journal of Heat and Mass Transfer*, 99:681-690. https://doi.org/10.1016/j.ijheatmasstransfer.2016.03.126

Fang XD, Zhuang FT, Chen C, et al., 2019. Saturated flow boiling heat transfer: review and assessment of prediction methods. *Heat and Mass Transfer*, 55(1):197-222. https://doi.org/10.1007/s00231-018-2432-1

Fu X, Qi SL, Zhang P, et al., 2008. Visualization of flow boiling of liquid nitrogen in a vertical mini-tube. *International Journal of Multiphase Flow*, 34(4):333-351. https://doi.org/10.1016/j.ijmultiphaseflow.2007.10.014

Fu X, Zhang P, Huang CJ, et al., 2010. Bubble growth, departure and the following flow pattern evolution during flow boiling in a mini-tube. *International Journal of Heat and Mass Transfer*, 53(21-22):4819-4831. https://doi.org/10.1016/j.ijheatmasstransfer.2010.06.010

Harirchian T, Garimella SV, 2008. Microchannel size effects on local flow boiling heat transfer to a dielectric fluid. *International Journal of Heat and Mass Transfer*, 51(15-16):3724-3735. https://doi.org/10.1016/j.ijheatmasstransfer.2008.03.013

Hartwig J, Hu H, Styborski J, et al., 2015. Comparison of cryogenic flow boiling in liquid nitrogen and liquid hydrogen chilldown experiments. *International Journal of Heat and Mass Transfer*, 88:662-673. https://doi.org/10.1016/j.ijheatmasstransfer.2015.04.102

Hartwig J, Darr S, Asencio A, 2016. Assessment of existing two phase heat transfer coefficient and critical heat flux correlations for cryogenic flow boiling in pipe quenching experiments. *International Journal of Heat and Mass Transfer*, 93:441-463. https://doi.org/10.1016/j.ijheatmasstransfer.2015.09.028

Huang Q, Jia L, Dang C, et al., 2018. Experimental study on flow boiling of deionized water in a horizontal long small channel. *Journal of Thermal Science*, 27(2):157-166. https://doi.org/10.1007/s11630-018-0996-1

Huo X, Chen L, Tian YS, et al., 2004. Flow boiling and flow regimes in small diameter tubes. *Applied Thermal Engineering*, 24(8-9):1225-1239. https://doi.org/10.1016/j.applthermaleng.2003.11.027

Hurlbert EA, Whitley R, Klem MD, et al., 2016. International space exploration coordination group assessment of technology gaps for LO_x/methane propulsion systems for the global exploration roadmap. AIAA SPACE Forum. https://doi.org/10.2514/6.2016-5280

Huzel DK, Huang DH, 1992. Modern Engineering for Design of Liquid-propellant Rocket Engines. AIAA, Washington DC, USA. https://doi.org/10.2514/4.866197

Karayiannis TG, Mahmoud MM, 2017. Flow boiling in microchannels: fundamentals and applications. *Applied Thermal Engineering*, 115:1372-1397. https://doi.org/10.1016/j.applthermaleng.2016.08.063

Kim SM, Mudawar I, 2013. Universal approach to predicting saturated flow boiling heat transfer in mini/micro-channels–part II. Two-phase heat transfer coefficient. *International Journal of Heat and Mass Transfer*, 64:1239-1256. https://doi.org/10.1016/j.ijheatmasstransfer.2013.04.014

Kim SM, Mudawar I, 2014. Review of databases and predictive methods for heat transfer in condensing and boiling mini/micro-channel flows. *International Journal of Heat and Mass Transfer*, 77:627-652. https://doi.org/10.1016/j.ijheatmasstransfer.2014.05.036

Klem MD, Smith T, Wadel M, et al., 2011. Liquid oxygen/liquid methane propulsion and cryogenic advanced development. Proceedings of the 62nd International Aeronautical Congress.

Klimenko VV, 1982. Heat transfer intensity at forced flow boiling of cryogenic liquids in tubes. *Cryogenics*, 22(11):569-576. https://doi.org/10.1016/0011-2275(82)90003-0

Klimenko VV, Sudarchikov AM, 1983. Investigation of forced flow boiling of nitrogen in a long vertical tube. *Cryogenics*, 23(3):379-385.

Laverty WF, Rohsenow WM, 1964. Film Boiling of Saturated Liquid Flowing Upward Through a Heated Tube: High Vapor Quality Range. MIT, Cambridge, USA.

Lee S, Devahdhanush VS, Mudawar I, 2018. Investigation of subcooled and saturated boiling heat transfer mechanisms, instabilities, and transient flow regime maps for large

length-to-diameter ratio micro-channel heat sinks. *International Journal of Heat and Mass Transfer*, 123: 172-191. https://doi.org/10.1016/j.ijheatmasstransfer.2018.02.020

Li W, Li JY, Feng ZZ, et al., 2017. Local heat transfer in subcooled flow boiling in a vertical mini-gap channel. *International Journal of Heat and Mass Transfer*, 110: 796-804. https://doi.org/10.1016/j.ijheatmasstransfer.2017.03.086

Liu JY, Liu JP, Li RX, et al., 2018. Experimental study on flow boiling characteristics in a high aspect ratio vertical rectangular mini-channel under low heat and mass flux. *Experimental Thermal and Fluid Science*, 98:146-157. https://doi.org/10.1016/j.expthermflusci.2018.05.019

Liu XF, Chen XY, Zhang QY, et al., 2017. Investigation on CHF of saturated liquid nitrogen flow boiling in a horizontal small channel. *Applied Thermal Engineering*, 125: 1025-1036. https://doi.org/10.1016/j.applthermaleng.2017.07.018

Mercado M, Wong N, Hartwig J, 2019. Assessment of two-phase heat transfer coefficient and critical heat flux correlations for cryogenic flow boiling in pipe heating experiments. *International Journal of Heat and Mass Transfer*, 133:295-315. https://doi.org/10.1016/j.ijheatmasstransfer.2018.12.108

Qi SL, 2007. Flow and Heat Transfer of Liquid Nitrogen in Micro-tubes. PhD Thesis, Shanghai Jiao Tong University, Shanghai, China (in Chinese).

Qi SL, Zhang P, Wang RZ, et al., 2007a. Flow boiling of liquid nitrogen in micro-tubes: Part I–the onset of nucleate boiling, two-phase flow instability and two-phase flow pressure drop. *International Journal of Heat and Mass Transfer*, 50(25-26):4999-5016. https://doi.org/10.1016/j.ijheatmasstransfer.2007.08.018

Qi SL, Zhang P, Wang RZ, et al., 2007b. Flow boiling of liquid nitrogen in micro-tubes: Part II–heat transfer characteristics and critical heat flux. *International Journal of Heat and Mass Transfer*, 50(25-26):5017-5030. https://doi.org/10.1016/j.ijheatmasstransfer.2007.08.017

Qu WL, Mudawar I, 2003. Flow boiling heat transfer in two-phase micro-channel heat sinks–I. Experimental investigation and assessment of correlation methods. *International Journal of Heat and Mass Transfer*, 46(15): 2755-2771. https://doi.org/10.1016/S0017-9310(03)00041-3

Ribatski G, Wojtan L, Thome JR, 2006. An analysis of experimental data and prediction methods for two-phase frictional pressure drop and flow boiling heat transfer in micro-scale channels. *Experimental Thermal and Fluid Science*, 31(1):1-19. https://doi.org/10.1016/j.expthermflusci.2006.01.006

Sandler S, Zajaczkowski B, Krolicki Z, 2018. Review on flow boiling of refrigerants R236fa and R245fa in mini and micro channels. *International Journal of Heat and Mass Transfer*, 126:591-617. https://doi.org/10.1016/j.ijheatmasstransfer.2018.05.048

Sempértegui-Tapia DF, Ribatski G, 2017. Flow boiling heat transfer of R134a and low GWP refrigerants in a horizontal micro-scale channel. *International Journal of Heat and Mass Transfer*, 108:2417-2432. https://doi.org/10.1016/j.ijheatmasstransfer.2017.01.036

Shah MM, 1976. A new correlation for heat transfer during boiling flow through pipes. *ASHRAE Transactions*, 82: 66-86.

Shahmardan MM, Norouzi M, Kayhani MH, et al., 2012. An exact analytical solution for convective heat transfer in rectangular ducts. *Journal of Zhejiang University-SCIENCE A (Applied Physics & Engineering)*, 13(10): 768-781.

Steiner D, 1986. Heat transfer during flow boiling of cryogenic fluids in vertical and horizontal tubes. *Cryogenics*, 26(5): 309-318. https://doi.org/10.1016/0011-2275(86)90007-X

Steiner D, Schlünder EU, 1976. Heat transfer and pressure drop for boiling nitrogen flowing in a horizontal tube: 1. Saturated flow boiling. *Cryogenics*, 16(7):387-398. https://doi.org/10.1016/0011-2275(76)90050-3

Sutton GP, 2005. History of Liquid Propellant Rocket Engines. AIAA, Reston, USA. https://doi.org/10.2514/4.868870

Taylor JR, 1997. An Introduction to Error Analysis, 2nd Edition. University Science Books, Mill Valley, USA.

Thome JR, Consolini L, 2010. Mechanisms of boiling in micro-channels: critical assessment. *Heat Transfer Engineering*, 31(4):288-297. https://doi.org/10.1080/01457630903312049

Tibiriçá CB, Ribatski G, 2010. Flow boiling heat transfer of R134a and R245fa in a 2.3 mm tube. *International Journal of Heat and Mass Transfer*, 53(11-12):2459-2468. https://doi.org/10.1016/j.ijheatmasstransfer.2010.01.038

Tran TN, Wambsganss MW, France DM, 1996. Small circular- and rectangular-channel boiling with two refrigerants. *International Journal of Multiphase Flow*, 22(3):485-498. https://doi.org/10.1016/0301-9322(96)00002-X

Umekawa H, Ozawa M, Yano T, 2002. Boiling two-phase heat transfer of LN_2 downward flow in pipe. *Experimental Thermal and Fluid Science*, 26(6-7):627-633. https://doi.org/10.1016/S0894-1777(02)00181-4

Wang H, Fang XD, 2014. Review of correlations of flow boiling heat transfer coefficients for nitrogen. Proceedings of the 12th International Conference on Nanochannels, Microchannels, and Minichannels collocated with the ASME 2014 4th Joint US-European Fluids Engineering Division Summer Meeting. https://doi.org/10.1115/ICNMM2014-21212

Wang Y, Sefiane K, 2012. Effects of heat flux, vapour quality, channel hydraulic diameter on flow boiling heat transfer in variable aspect ratio micro-channels using transparent heating. *International Journal of Heat and Mass Transfer*, 55(9-10):2235-2243.

https://doi.org/10.1016/j.ijheatmasstransfer.2012.01.044

Yang CY, Nalbandian H, Lin FC, 2018. Flow boiling heat transfer and pressure drop of refrigerants HFO-1234yf and HFC-134a in small circular tube. *International Journal of Heat and Mass Transfer*, 121:726-735. https://doi.org/10.1016/j.ijheatmasstransfer.2017.12.161

Yu ZJ, 2012. Study on Flow Friction and Characteristics of Heat Transfer of Liquid Nitrogen Boiling Two-phase in Vertical Circular Tube. MS Thesis, Shanghai Jiao Tong University, Shanghai, China (in Chinese).

Zhang P, Fu X, 2009. Two-phase flow characteristics of liquid nitrogen in vertically upward 0.5 and 1.0 mm micro-tubes: visualization studies. *Cryogenics*, 49(10):565-575. https://doi.org/10.1016/j.cryogenics.2008.10.017

Zhang QY, Chen J, Li JP, et al., 2017. Experimental study on saturated flow boiling heat transfer of nitrogen in a small-diameter horizontal heated tube. *Experimental Thermal and Fluid Science*, 86:257-271. https://doi.org/10.1016/j.expthermflusci.2017.04.003

中文概要

题　目： 单个微小通道中液氮流动沸腾换热实验研究

目　的： 面向液体火箭发动机再生冷却，针对较高亚临界压力下单个垂直微小通道中液氮的流动沸腾传热特性开展实验研究，讨论并分析热流密度、密流和入口压力对沸腾曲线和局部换热系数的影响，以获得液氮在微小通道中较高亚临界压力下的流动沸腾传热机理及实验关系式。

创新点： 1. 通过工况参数对沸腾曲线和局部换热系数的影响分析，得到液氮在微小通道中较高亚临界压力下的流动沸腾传热机理；2. 提出微小通道中较高亚临界压力下的流动沸腾传热修正关系式。

方　法： 1. 通过实验方法，得到液氮在微小通道中较高亚临界压力下的沸腾曲线和局部换热系数；2. 通过实验与理论分析相结合，得到液氮在微小通道中较高亚临界压力下的流动沸腾传热机理；3. 通过理论分析，将实验结果与六种预测关系式进行比较，并根据实验数据提出一种改进的实验关系式（表 7）。

结　论： 1. 热流密度对换热系数有较大影响，随着热流密度的增大，出现了三种变化趋势；2. 在实验范围内，密流的增大抑制了核态沸腾，并且降低了环状流的局部换热系数；3. 入口压力的增大在较大干度范围内增大了局部换热系数，直到局部蒸干的出现；4. 综合考虑核态沸腾和局部蒸干两种主导传热机理，在 Tran 关系式的基础上提出了一种适用于较高亚临界压力条件下微小通道中液氮流动沸腾的修正实验关系式（平均绝对误差为 19.3%）。

关键词： 微小通道；液氮；流动沸腾；传热；再生冷却